Title

Organoid models of human and mouse ductal pancreatic cancer.

Journal

Cell, 160(1-2)

ISSN

0092-8674

Authors

Boj, Sylvia F

Hwang, Chang-Il

Baker, Lindsey A

et al.

Publication Date

2015

DOI

10.1016/j.cell.2014.12.021

Peer reviewed

Published in final edited form as:
Cell. 2015 January 15; 160(0): 324–338. doi:10.1016/j.cell.2014.12.021.

Organoid Models of Human and Mouse Ductal Pancreatic Cancer

Sylvia F. Boj[1,2,15], **Chang-Il Hwang**[3,4,15], **Lindsey A. Baker**[3,4,15], **Iok In Christine Chio**[3,4,15], **Dannielle D. Engle**[3,4,15], **Vincenzo Corbo**[3,4,15], **Myrthe Jager**[1,15], **Mariano Ponz-Sarvise**[3,4], **Hervé Tiriac**[3,4], **Mona S. Spector**[3,4], **Ana Gracanin**[1,2], **Tobiloba Oni**[3,4,5], **Kenneth H. Yu**[3,4,6,7], **Ruben van Boxtel**[1], **Meritxell Huch**[1,8], **Keith D. Rivera**[3], **John P. Wilson**[3], **Michael E. Feigin**[3,4], **Daniel Öhlund**[3,4], **Abram Handly-Santana**[4,9], **Christine M. Ardito-Abraham**[3,4], **Michael Ludwig**[3,4], **Ela Elyada**[3,4], **Brinda Alagesan**[3,4,10], **Giulia Biffi**[3,4], **Georgi N. Yordanov**[4,9], **Bethany Delcuze**[3,4], **Brianna Creighton**[3,4], **Kevin Wright**[3,4], **Youngkyu Park**[3,4], **Folkert H.M. Morsink**[11], **I. Quintus Molenaar**[12], **Inne H. Borel Rinkes**[12], **Edwin Cuppen**[1], **Yuan Hao**[3], **Ying Jin**[3], **Isaac J. Nijman**[1], **Christine Iacobuzio-Donahue**[6], **Steven D. Leach**[6], **Darryl J. Pappin**[3], **Molly Hammell**[3], **David S. Klimstra**[13], **Olca Basturk**[13], **Ralph H. Hruban**[14], **George Johan Offerhaus**[11], **Robert G.J. Vries**[1,2], **Hans Clevers**[1,*], and **David A. Tuveson**[3,4,6,*]

[*]Correspondence: h.clevers@hubrecht.eu; dtuveson@cshl.edu.
[8]Current address: Gurdon Institute-University of Cambridge, Tennis Court Road Cambridge, CB2 1QN, UK
[15]Co-first authors

Conflicts of interest:
Dr. Ralph Hruban receives royalty payments from Myriad Genetics for the PalB2 inventions.
Dr. Hans Clevers and Meritxell Huch have patents pending and granted on the organoid technology.

Author contributions:
SFB: Initiated project, developed the methods for isolating mouse and human organoids, characterized human organoids: Figures 1A, 3, 4B, 4D, S4C, Tables S3 and S4.
CH: Developed transplantation models for organoids, performed shRNA knockdown, histological and karyotypic analyses: Figures 1A, 1E, 1G, 2A, 2C–E, 4D, 7; S1A–C, S2A–F, S2H, S4A–B, S7A–B; Tables S1, S2, S4.
LAB: Performed RNA-sequencing on mouse organoids, analyzed RNA-seq and proteomic data: Figures 5, 6, S5B, S6; Tables S5, S6, S7
IICC: Proteomic evaluation of mouse organoids, analyzed proteomic data: Figure 6.
DDE: Developed mouse organoid methods and evaluated CA19-9 levels in human organoids: Figures 1A, 2A, 4C, S3, S6, Table S6.
VC: Developed human organoid methods, performed molecular analyses of organoids, prepared material for DNA-sequencing, sequencing of Kras: Figures 1C–D, 3A, 3D, 4A, S1D–F, S5A; Table S3, S4, S5.
MJ: DNA-sequencing of human organoids: Figure 3D, Table S4.

Other contributors:
Mouse and human organoid preparation and characterization: MPS, HT, MSS, TO, DÖ, AHS, CMAA, ML, EE, BA, MEF, GY, GB, BD, BC, KW, KHY, YP, EC, MH, AG, RVB, FHMM, SL
Sequencing analyses: YH, YJ, MH, IN
Pathological analyses: GJO, RHH, DK, OB, CID
Surgical resections and tissue dissection: IQM, IHBR
Proteomic development: DJP, KDR, JPW
Overall study management: DAT, HC, RGJV
Manuscript writing: SFB, DDE, LAB, MEF, CH, HT, VC, MPS, RGJV, HC, IICC, DAT

[1]Hubrecht Institute, Royal Netherlands Academy of Arts and Sciences (KNAW), University Medical Centre Utrecht and CancerGenomics.nl, 3584CT Utrecht, the Netherlands. Cancer GenomiCs.nl [2]foundation Hubrecht Organoid Technology (HUB), Upsalalaan 8, 3584CT, Utrecht, the Netherlands [3]Cold Spring Harbor Laboratory, Cold Spring Harbor, NY 11724, USA [4]Lustgarten Pancreatic Cancer Research Laboratory, Cold Spring Harbor, NY 11724, USA [5]Graduate Program in Molecular and Cellular Biology, Stony Brook University, Stony Brook, NY 11794, USA [6]Rubenstein Center for Pancreatic Cancer Research, Memorial Sloan Kettering Cancer Center, New York, NY 10065, USA [7]Weill Medical College at Cornell University, New York, NY 10065, USA [9]Watson School of Biological Sciences, Cold Spring Harbor Laboratory, Cold Spring Harbor, NY 11724, USA [10]Graduate Program in Genetics, Stony Brook University, Stony Brook, NY 11794, USA [11]Department of Pathology, University Medical Centre Utrecht, 3584 CX Utrecht, The Netherlands [12]Department of Surgery, University Medical Center Utrecht, 3584 CX Utrecht, The Netherlands [13]Department of Pathology, Memorial Sloan Kettering Cancer Center, New York, NY 10065, USA [14]The Sol Goldman Pancreatic Cancer Research Center, Johns Hopkins University School of Medicine, Baltimore, MD 21231, USA

SUMMARY

Pancreatic cancer is one of the most lethal malignancies due to its late diagnosis and limited response to treatment. Tractable methods to identify and interrogate pathways involved in pancreatic tumorigenesis are urgently needed. We established organoid models from normal and neoplastic murine and human pancreas tissues. Pancreatic organoids can be rapidly generated from resected tumors and biopsies, survive cryopreservation and exhibit ductal- and disease stage-specific characteristics. Orthotopically transplanted neoplastic organoids recapitulate the full spectrum of tumor development by forming early-grade neoplasms that progress to locally invasive and metastatic carcinomas. Due to their ability to be genetically manipulated, organoids are a platform to probe genetic cooperation. Comprehensive transcriptional and proteomic analyses of murine pancreatic organoids revealed genes and pathways altered during disease progression. The confirmation of many of these protein changes in human tissues demonstrates that organoids are a facile model system to discover characteristics of this deadly malignancy.

INTRODUCTION

Mortality due to pancreatic cancer is projected to surpass that of breast and colorectal cancer by 2030 in the United States (Rahib et al., 2014; Siegel et al., 2013). This dire scenario reflects an aging population, the improvement of outcomes for breast and colorectal cancer patients, the advanced stage at which most patients with pancreatic cancer are diagnosed, and the lack of durable treatment responses in pancreatic cancer patients. Indeed, effective therapeutic strategies for patients with pancreatic ductal adenocarcinoma (PDA) have been difficult to identify (Abbruzzese and Hess, 2014).

The therapeutic resistance of PDA has been explored in a variety of cell culture and animal model systems, with clinically actionable findings encountered only occasionally (Villarroel et al., 2011). Patient derived xenografts (PDXs) have yielded insights into PDA, but their

generation requires a large amount of tissue and takes multiple months to establish (Kim et al., 2009; Rubio-Viqueira et al., 2006). Genetically engineered mouse models (GEMMs) of PDA have also been generated as a parallel system to investigate fundamental biology and clinical implications (Perez-Mancera 2012). These GEMMs accurately mimic the pathophysiological features of human PDA, including disease initiation from pre-invasive pancreatic intraepithelial neoplasms (PanINs) (Hingorani et al., 2003; Perez-Mancera et al., 2012), and were used to discover that PDA possesses a deficient vasculature that impairs drug delivery (Erkan et al., 2009; Jacobetz et al., 2012; Koong et al., 2000; Olive et al., 2009; Provenzano et al., 2012). While GEMMs have informed PDA therapeutic development (Beatty et al., 2011; Frese et al., 2012; Neesse et al., 2014), they are expensive and time-consuming (Perez-Mancera et al., 2012). In addition, both human PDA and GEMMs exhibit an extensive stromal component that decreases the neoplastic cellularity, making it difficult to isolate and characterize the epithelium-derived malignant cells in murine pancreatic neoplastic tissues.

To study neoplastic cells, dissociated human tumors are often grown in two-dimensional (2D) culture conditions (Sharma et al., 2010), which do not support growth of untransformed, non-neoplastic pancreatic cells. Three-dimensional (3D) culture strategies have been developed to study normal, untransformed cells, but only allow minimal propagation (Agbunag and Bar-Sagi, 2004; Lee et al., 2013; Means et al., 2005; Rovira et al., 2010; Seaberg et al., 2004). A comprehensive 3D cell culture model of murine and human PDA progression would facilitate investigation of genetic drivers, therapeutic targets, and diagnostics for PDA.

To address this deficiency, we sought to generate normal and neoplastic pancreatic organoids by modifying approaches we previously pioneered to culture intestinal (Sato et al., 2009), gastric (Barker et al., 2010), colon carcinoma (Sato et al., 2011), hepatic (Huch et al., 2013b), pancreatic (Huch et al., 2013a), and prostatic organoids (Gao et al., 2014; Karthaus et al., 2014). We developed 3D organoids from normal and malignant murine pancreatic tissues and used this model system to investigate PDA pathogenesis. Pancreatic organoids derived from wild-type mice and PDA GEMMs accurately recapitulate physiologically relevant aspects of disease progression *in vitro*. Following orthotopic transplantation, organoids from wild-type mouse normal pancreata are capable of regenerating normal ductal architecture, unlike other 3D model systems. We further developed methods to generate pancreatic organoids from normal and diseased human tissues, as well as from endoscopic needle biopsies. Following transplantation, organoids derived from murine and human PDA generate lesions reminiscent of PanIN and progress to invasive PDA. Finally, we demonstrate the utility of organoids to identify molecular pathways that correlate with disease progression, and that represent therapeutic and diagnostic opportunities.

RESULTS

Murine pancreatic ductal organoids expressing oncogenic Kras recapitulate features of PanINs

Recently, we derived continuously proliferating, normal pancreatic organoids from adult murine ductal cells (Huch et al., 2013a). We optimized this approach to generate models of PDA progression. We manually isolated small intralobular ducts and established organoid cultures from C57Bl/6 mouse normal pancreata and pancreatic tissues that contained low-grade murine PanIN (mPanIN-1a/b) from *Kras*$^{+/LSL\text{-}G12D}$; *Pdx1-Cre* ("KC") mice (Figure 1A). KC mice develop a spectrum of pre-invasive ductal lesions that mirror human PanINs, and upon aging, stochastically develop primary and metastatic PDA (Hingorani et al., 2003). Ducts from KC pancreata were often larger and exhibited higher grades of dysplasia compared to those from wild-type mice (Figure 1A). After 1–3 days in culture, organoid growth was observed from isolated ducts (Figure 1A). We created a collection of 10 murine normal (mN) and 9 PanIN (mP) organoid cultures that we have continuously propagated for over 20 passages and successfully cryopreserved (Table S1A). mP organoids exhibited recombination of the conditional *Kras*$^{LSL\text{-}G12D}$ allele and higher levels of Kras-GTP when compared to mN organoids (Figure 1B).

To determine the contribution of different pancreatic lineages to the organoids, we evaluated the expression of pancreatic lineage markers in organoids. Genes associated with the ductal lineage (*Ck19*, *Sox9*) (Cleveland et al., 2012) were enriched in the mN and mP organoids compared to total pancreatic tissues which contain relatively few ductal cells (Figure 1C). In addition, the mP organoids up-regulated genes indicative of a PanIN disease state (*Muc5ac*, *Muc6*, *Tff1*) relative to mN, with no difference in *Klf4* (Figure 1D) (Prasad et al., 2005). GFP-transduced mN and mP organoids were orthotopically transplanted into syngeneic C57Bl/6 or *Nu/Nu* mice. mN organoids quickly formed ductal structures comprised of simple cuboidal cells that persisted for up to one month (n = 9/27 transplants), but were not observed after 2 months (n = 0/13 transplants) (Figure 1E, Table S1B). In comparison, mP organoids formed small cysts lined with a single layer of simple cuboidal ductal cells interspersed with mucin-containing columnar epithelial cells. Although we could not demonstrate that the mP transplants were contiguous with the native ductal system, they resembled pre-invasive mPanIN (Figure S1C). These dysplastic epithelial cells persisted for 2 months or longer (n = 16/18 transplants), were GFP and Ck19 positive, expressed the mPanIN-associated mucin Muc5ac, and stained prominently with Alcian Blue (Figure 1E, Table S1C). In addition, dysplastic cells had increased proliferation and a robust stromal response when compared to mN transplants, both of which are characteristic of autochthonous mPanIN tissue (Figures S1A–C). The ability of transplanted mP organoids to form lesions with many of the features of mPanINs demonstrates the utility of this system as a model for early pancreatic neoplasia.

Multiple cellular origins have been proposed for the development of PDA, with the pancreatic acinar cell hypothesized to be a major contributor to PDA initiation (De La et al., 2008; Gidekel Friedlander et al., 2009; Guerra et al., 2003; Habbe et al., 2008; Kopp et al., 2012; Morris et al., 2010; Sawey et al., 2007). However, recent studies have suggested that

transformation of pancreatic ductal cells can also give rise to PDA (Pylayeva-Gupta et al., 2012; Ray et al., 2011; von Figura et al., 2014). Acinar cells isolated from wild-type pancreata are unable to form organoids in our conditions (Huch et al., 2013a). Therefore, our pancreatic ductal organoid system offers a unique opportunity to determine whether ductal cells can give rise to mPanIN. To assess whether expression of oncogenic Kras in pancreatic ductal organoids is sufficient to induce mPanIN formation *in vivo*, we derived organoids from ducts harboring the conditional $Kras^{+/LSL\text{-}G12D}$ allele (Hingorani et al., 2003). Following activation of Kras by adenoviral-*Cre* (Ad-*Cre*) infection, $Kras^{G12D}$ organoids maintained expression of genes specific to ductal cells and not acinar or endocrine lineages (Figures S1D and S1E). Recombination of the $Kras^{+/LSL\text{-}G12D}$ allele was confirmed by PCR, and levels of GTP-bound Kras were increased relative to control-infected organoids (Figure 1F). In addition, expression of $Kras^{G12D}$ resulted in the up-regulation of genes associated with human PanIN (Figure S1F). The $Kras^{G12D}$-expressing organoids demonstrated increased proliferation relative to control organoids (Figure S1G). Finally, $Kras^{G12D}$ organoids formed mPanIN-like structures with columnar cell morphology when implanted orthotopically into syngeneic mice (Figure 1G). This morphology contrasted with the normal-appearing ductal architecture formed by transplanting $Kras^{+/LSL\text{-}G12D}$ organoids or wild-type mN organoids (Figures 1E and 1G). The ability of mPanIN-like structures to develop from $Kras^{G12D}$-expressing ductal organoids following transplantation demonstrates that ductal cells are also competent to form mPanINs.

Tumor-derived organoids provide a model for murine PDA progression

We prepared pancreatic ductal organoids from multiple murine primary tumors (mT) and metastases (mM) from KC and *Kras*$^{+/LSL\text{-}G12D}$; *Trp53*$^{+/LSL\text{-}R172H}$; *Pdx-Cre* (“KPC”) mice which develop mPDA more rapidly than KC mice (Figure 2A, Table S2A) (Hingorani et al., 2005). mT and mM organoids exhibited recombination of the *Kras* $^{LSL\text{-}G12D}$ allele, increased levels of Kras-GTP and Kras protein (Figure 2B). mT and mM organoids had an increased level in S6 phosphorylation, but not Erk or Akt phosphorylation (Figure 2B).

Orthotopic transplantation of mT organoids initially generated low- and high-grade lesions that resembled mPanIN (Figure 2C, Table S2B). Over longer periods of time (1 – 6 months), transplants developed into invasive primary and metastatic mPDA (Figure 2C, Table S2B). mT organoids engrafted with a similar efficiency upon orthotopic transplantation in *Nu/Nu* mice (91.7%) compared to C57Bl/6 mice (85%), but disease progression was accelerated in *Nu/Nu* hosts (Table S2B). While most mT organoid transplants required several months to progress from early mPanIN-like lesions to invasive and metastatic cancer (Figure 2C, Table S2B), mM organoids rapidly formed invasive mPDA within 1 month (Table S2C). The ability of organoid transplants to reproduce the discrete stages of disease progression contrasts with the rapid formation of advanced mPDA following transplantation of 2D cell lines (Figure S2A–C) (Olive et al., 2009).

The tumor exhibited a prominent stromal response in the transplanted mT and mM organoids and resembled autochthonous tumors from KPC mice (Figure S2A) (Olive et al., 2009). This stromal response is often absent in tumors formed from 2D cell lines (Figure S2A) (Olive et al., 2009). Low vascular density and high vessel-to-tumor distance were also

observed, demonstrating the close resemblance of the organoid transplantation models to autochthonous mPDA, in contrast to transplanted 2D cell lines (Figure S2A–C) (Olive et al., 2009).

Loss of heterozygosity (LOH) for *Trp53* has been reported as a common feature of mPDA based on studies of 2D cell lines (Hingorani et al., 2005). Therefore, we assayed for *Trp53* LOH in our murine 3D organoids. All mT organoids prepared from KPC tumors maintained expression of p16, did not exhibit *Trp53* LOH and maintained a stable karyotype, whereas most mM organoids lost the wild-type *Trp53* allele and were aneuploid (Figures 2D, 2E and S2D). We generated 2D cell lines from mT and mM organoids, but found that mN and mP organoids were unable to propagate in 2D. mT1 was derived from a KC mouse PDA, lacks the mutant *Trp53* allele and was also unable to propagate in 2D. All mT-derived 2D cell lines exhibited*Trp53* LOH and were aneuploid (Figure 2E and S2D).

To determine whether organoids are suitable for genetic cooperation experiments, shRNAs targeting p53 and p16/p19 were introduced into mP organoids (Figure S2E). While the proliferation of mP organoids increased upon knockdown of either p53 or p16/p19 (Figure S2G), only p53 knockdown enabled 2D growth and colony formation (Figure S2F, **data not shown**). Also, only p53 knockdown promoted progression of mP organoid transplants to invasive carcinoma within 3 months (Figure S2H). This contrasts with a previous report that biallelic loss of p16/p19 and Kras mutation promoted mPDA (Aguirre et al., 2003; Bardeesy et al., 2006), and may reflect differences in the genetic system or the initiating cellular compartment. Nevertheless, the cooperation between p53 depletion and oncogenic Kras demonstrates that organoids are a facile system to evaluate genetic mediators of PDA progression.

Human pancreatic organoids model PanIN to PDA progression

We modified our culture conditions to support the propagation of human normal and malignant pancreatic tissues. Isolation of ductal fragments was not always feasible because some normal pancreatic tissue samples were pre-digested in preparation for islet transplantation. Therefore, we directly embedded digested material into Matrigel. This approach achieved an isolation efficiency of 75–80% for human normal (hN) organoids (Figure 3A and S3, Table S3). hN organoids require TGF-beta pathway inhibitors (A83-01 and Noggin), R-Spondin1 and Wnt3a-conditioned media, EGF, and PGE2 for propagation (Figures 3B and 3C). Unlike mN organoids, which have unlimited propagation in culture, hN organoids ceased proliferating after 20 passages or approximately 6 months, but could be cryopreserved.

We modified the methods described above to accommodate the extensive desmoplastic reaction in freshly resected PDA specimens and generated human tumor-derived organoids (hT) (Figures 3A and S3). hT organoids could be passaged indefinitely and cryopreserved (Figure 3C). The establishment hT organoids had efficiencies of 75% (n = 3/4) and 83% (n = 5/6) in the Netherlands and USA, respectively (Table S3). The first specimen that failed to generate an organoid culture was obtained from a patient that had undergone neo-adjuvant chemotherapy, and histologic examination of this specimen revealed extensive necrosis. The second specimen that did not generate an organoid culture was predominantly composed of

stromal cells, without sufficient viable tumor cells to establish a culture. While the hN organoids had a simple, cuboidal morphology, the hT organoids had differing degrees of dysplastic tall columnar cells, resembling low-grade PanINs (Figures 3A). hT organoids tolerated the withdrawal of certain growth factors from the media (Figures 3B and 3C).

85% of pancreatic cancer patients are ineligible for surgical resection of their tumors (Ryan et al., 2014). Therefore, we determined whether hT organoids could be generated from the limited amount of cellular material provided by endoscopic biopsies using fine needle aspirations (FNA). Initial attempts to generate organoids from FNA biopsies were hampered by loss of cellular material during digestion. Upon optimization of these conditions, human FNA biopsy organoids (hFNA) were generated from two specimens that were not dissociated prior to suspension in Matrigel (Figures 3A and S3). This approach is broadly applicable to PDA patients and enables serial sampling.

Targeted sequencing of 2,000 cancer-associated genes was performed on hN and hT organoids. As expected, no mutations were detected in the hN organoid cultures. These analyses identified oncogenic *KRAS* mutations in the majority of tumor-derived samples (n = 8), and mutations in *TP53* (n = 7), *SMAD4* (n = 5), and *CDKN2A* (n = 4) (Figure 3D, Table S4). We also noted amplification of known oncogenes, such as *MYC* (n = 4), and loss of tumor suppressors, including *TGFBR2* (n = 3) and *DCC* (n = 5). Importantly, the same *KRAS* mutations observed in several hT organoids were confirmed in the primary PDA from which they were derived (Table S4). The allele frequency of oncogenic *KRAS* variants in hT1 – hT5 and hFNA2 ranged from approximately 50 - 100%. In contrast, the $KRAS^{G12V}$ allele frequency in hFNA1 was only 1% (Table S4), which may result from co-existence of wild-type ductal cells. While *KRAS* mutations were not detected in hT8 (Figure 3D, Table S4), the presence of mutations in known PDA genes (*ARID1A* and *MLL3*) suggests that hT8 contains malignant cells despite the absence of a *KRAS* mutation (Table S4).

To further characterize the cell types present in primary PDA organoids, we evaluated the expression of pancreatic lineage markers. hN and hT organoids expressed markers of ductal cells but not other pancreatic lineages (Figure 4A). The karyotypes of hT organoids were highly aneuploid, whereas the hN organoids were predominantly and stably diploid (Figure 4B). The PDA-associated biomarker CA19-9 (Makovitzky, 1986) was also elevated in hT relative to hN organoids (Figure 4C). The hN and hT organoids are therefore reflective of normal and neoplastic human pancreatic ductal cells and offer a model system to explore pancreatic cancer biology in the more genetically complex background of human cancer.

Following orthotopic transplantation into *Nu/Nu* mice, hN organoids produced normal ductal structures at low efficiency (n = 2/23), while hT organoids efficiently generated a spectrum of low and high-grade, extra-ductal PanIN-like lesions within one month (n = 9/12) (Figures 4D, S4A, Table S4). The hT-derived transplants initially formed well-defined hollow lesions lined by a single layer of columnar epithelial cells with apical mucin, and basally located, relatively uniform nuclei. The nuclei were small and lacked the pleomorphism and hyperchromasia often seen in invasive PDA. These lesions progressed over several months to infiltrative carcinoma comprised of poorly defined and invasive glands (Figures 4D, S4A, Table S4). A prominent desmoplastic reaction was present in hT-derived PanIN-like

structures and PDA, including the deposition of a collagen-rich stroma and the recruitment of αSMA-positive cells (Figure S4B). The mutation or loss of *TP53* or *SMAD4* in hT1 and hT2 was also detected by IHC in these tumors (Figure S4C, Table S4). Overall, hT organoids represent a transplantable model of human pancreatic cancer progression.

Gene expression analysis of murine pancreatic ductal organoids implicates candidate genes in PDA progression

The mouse organoids were prepared from syngeneic mice, offering the ability to discern gene expression changes in organoids and determine whether these changes correlate with PDA progression. We harvested RNA from mN (n = 7), mP (n = 6), and mT (n = 6) organoids and generated strand-specific RNA-sequencing (RNA-seq) libraries. Sequences were mapped to the mm9 version of the mouse genome, and relative transcript abundances (transcripts per million) of 29,777 mouse genes were determined (Table S5). Principal component analysis revealed that mN organoids were distinct from mP and mT organoids (Figure 5A and Table S5).

Genes whose levels differed significantly among mN, mP, and mT organoids were identified. 772 genes were found down-regulated and 863 genes up-regulated in mP relative to mN organoids (Figure 5B and Table S5). When mT organoids were compared to mN organoids, 2,721 genes were down-regulated and 2,695 up-regulated. In addition, 823 genes were down-regulated and 640 genes up-regulated in mT relative to mP organoids. Distinct patterns of gene expression were found in the dataset (Figure 5C). The majority of genes differentially expressed in mP relative to mN organoids changed in a similar manner in mT relative to mN organoids (Figure 5D). However, a much larger cohort of genes changed in expression in mT relative to mN than in mP relative to mN organoids (Figure 5D), suggesting that mP organoids represent an intermediate state between mN and mT organoids.

The glycosyltransferase *Gcnt3* and putative protein disulfide isomerase *Agr2* were among the most up-regulated genes in both mP and mT organoids, and have been demonstrated to be elevated in human PDA (Figure 5E) (Dumartin et al., 2011; Zhao et al., 2014). The most up-regulated gene in both mP and mT relative to mN organoids was the acyl-CoA synthetase *Acsm3* (Figure 5E). RNA-seq results were confirmed by qRT-PCR for 35 out of 40 genes (Table S5), including the up-regulation of *Agr2*, *Acsm3*, *Gcnt1*, *Gcnt3*, and *Ugdh*, and the down-regulation of the *Ptprd* gene in mP and mT organoids (Figure 5F and Table S5). Among the genes up-regulated in mP and mT relative to mN organoids, *Gcnt1*, *Gcnt3*, *Acsm3*, *Agr2*, *Syt16*, *Nt5e*, and *Ugdh* were up-regulated following the Ad-Cre induced expression of oncogenic $Kras^{G12D}$, suggesting that these genes are activated downstream of mutant $Kras^{G12D}$ (Figure S5A). To determine whether organoid RNA-seq profiles resembled gene expression patterns *in vivo*, we compared our organoid RNA-seq data to a published transcription profile of murine pancreatic tumors upon $Kras^{G12D}$ inactivation (Ying et al., 2012). Genes differentially expressed upon oncogenic Kras activation overlapped significantly with those up or down-regulated in mP or mT relative to mN organoids (Figure S5B). These analyses demonstrate the ability of the organoid system to identify molecular alterations associated with PDA progression.

Proteomic alterations in murine pancreatic ductal organoids predict pathways associated with PDA progression

As an orthogonal method to investigate molecular alterations in murine pancreatic organoids, we characterized the global proteome of mN (n = 5), mP (n = 4) and mT (n = 5) organoids. Protein lysates were processed using amine-reactive isobaric tags for relative and absolute quantification (iTRAQ) mass spectrometry (Wiese et al., 2007). Samples were run in four 8-plex experiments and merged using an approach that normalizes the data to common samples included across all experiments (Supplemental Experimental Procedures). Upon merging, 6,051 unique protein isoforms were quantified in all samples. We applied linear regression modeling on the normalized intensity peak values and identified 710 protein isoform expression changes between mN and mP organoids (Figure 6A). 1,047 protein isoforms changed expression between mN and mT organoids, and 63 differentially expressed proteins were identified between mP and mT (Figure 6A). The relatively small number of protein expression changes identified between mP and mT organoids reflects the biological similarity between mP and mT (Figure S6A).

mN organoids showed unique proteomic profiles from their mP and mT counterparts (Figure 6B and 6C). To compare the proteomic and RNA-seq data, we collapsed the unique protein isoforms into their corresponding 4,155 genes. Some protein expression changes (e.g. 123/150 for down-regulated and 96/151 for up-regulated mP proteins) did not reflect corresponding transcriptional changes, indicating that protein stability may play a role in cancer progression, particularly in mP organoids (Figure 6D). Nonetheless, the proteomic data validated many of the expression changes identified by RNA-seq (Figure 6D), including up-regulation of Gcnt3, Agr2, and Ugdh (Table S6). Additionally, of the 1,599 genes whose expression levels changed in mT relative to mN organoids that were measured by mass spectrometry, 301 (19%) showed corresponding protein changes (Figure 6D).

Gene Set Enrichment Analysis (GSEA) on the RNA-seq and proteomic data (Subramanian et al., 2005) revealed elevated expression of genes and proteins involved in Glutathione Metabolism and Biological Oxidations in mP relative to mN organoids (Figures 6E, S6B, S6C, Table S7), consistent with elevations in reactive oxygen species metabolism previously reported in $Kras^{G12D}$ cells (DeNicola et al., 2011; Ying et al., 2012). The enrichment of proteins involved in Glutathione metabolism was also found in mT relative to mN organoids (Table S7). Additionally, we identified a significant positive enrichment of proteins involved in the Steroid Biosynthesis, Cholesterol Biosynthesis, One Carbon Pool by Folate, and Pyrimidine Metabolism pathways (Figures 6E, S6B, S6C, Table S7), consistent with an earlier report (Ying et al., 2012). Similar pathways were enriched in mP relative to mN organoids (Cholesterol Biosynthesis, One Carbon Pool by Folate, and Pyrimidine Metabolism) (Figures S6B and S6C, Table S7), while Fatty Acid Metabolism and TCA Cycle/Respiratory Electron Transport pathways were down-regulated (Figures S6B and S6C, Table S7). The increase in anabolic and decrease in catabolic pathways suggest that complex alterations in fatty acid metabolism occur during PDA progression.

Interestingly, we also found broad up-regulation of the nucleoporin family at both the RNA and protein levels in the mT relative to mN organoids (Figure 6F, Table S6). The individual

nucleoporins NUP214, NUP153 and NUPL1 were previously identified in shRNA dropout screens in pancreatic cancer cell lines (Cheung et al., 2011; Shain et al., 2013). Furthermore, amplification of NUP153 was detected in one human PDA cancer cell line, and elevation of NUP88 was detected in human primary PDA (Cheung et al., 2011; Gould et al., 2000; Shain et al., 2013). This systematic analysis of molecular alterations in pancreatic organoids implicates nuclear transport as a pathway correlated with pancreatic cancer progression.

In vivo mouse and human validation of candidates associated with PDA progression in organoids

To demonstrate that the mouse organoid culture system represents a biological resource for the accurate discovery of genes associated with PDA progression, we selected 16 genes up-regulated in mT organoids for validation in primary tissue specimens by IHC and immunofluorescence (IF) (Figure 7A). These 16 genes included enzymes, membrane proteins, structural proteins and secreted ligands, which could represent candidate biomarkers and therapeutic targets. Of the 14 antibodies that generated a detectable signal on murine pancreatic tissue sections, 13 antibodies confirmed the increased expression of the candidate protein in mPanIN and mPDA lesions in concordance with the RNA-seq and proteomic data (Figures 7A, 7B and S7A). 11 of the 13 candidate antibodies were compatible for evaluation in human tissues, and 7 of these candidates were up-regulated in human PDA when compared to normal pancreatic ductal tissues (Figures 7C, 7D and S7B). The high expression of many of these markers was recapitulated in orthotopic transplants of hT organoids into *Nu/Nu* mice (Figure 7C). These results indicate that the organoid culture system accurately models PDA progression and can serve as a resource for the discovery and genetic dissection of pathways driving human pancreatic tumorigenesis.

DISCUSSION

We have established pancreatic organoids as a tractable and transplantable system to probe the molecular and cellular properties of neoplastic progression in mice and humans. In contrast to prior reports (Agbunag and Bar-Sagi, 2004; Rovira et al., 2010; Seaberg et al., 2004), our culture conditions prevent the rapid exhaustion of normal ductal cells *in vitro*, and generate a normal ductal architecture following orthotopic transplantation. Importantly, the ability to passage and transplant both normal and neoplastic ductal cells enables a detailed analysis of molecular pathways and cellular biology that is not possible when neonatal pancreatic fragments are propagated in air-liquid interfaces, or induced pluripotent cells are employed (Agbunag and Bar-Sagi, 2004; Kim et al., 2013; Li et al., 2014). For example, our finding that nucleoporins are broadly up-regulated in the neoplastic murine organoids, coupled with the known associations of nucleoporins to cell proliferation and cell transformation, presents a class of proteins to investigate in pancreatic cancer progression (Gould et al., 2000; Kohler and Hurt, 2010). Furthermore, the ability to systematically characterize human pancreatic cancer organoids that lack KRAS mutations, such as hT8, will reveal driver genes for PDA. Finally, since organoids can be readily established from small patient biopsies, they should hasten the development of personalized approaches for pancreatic cancer patients.

EXPERIMENTAL PROCEDURES

Animals

Trp53$^{+/LSL\text{-}R172H}$, *Kras*$^{+/LSL\text{-}G12D}$ and *Pdx1-Cre* strains in C57Bl/6 background were interbred to obtain *Pdx1-Cre; Kras*$^{+/LSL\text{-}G12D}$ (KC) and *Pdx1-Cre; Kras*$^{+/LSL\text{-}G12D}$*; Trp53*$^{+/LSL\text{-}R172H}$ (KPC) mice (Hingorani et al., 2005). The *R26*$^{LSL\text{-}YFP}$ strain was interbred to get the desired genotype. C57Bl/6 and athymic *Nu/Nu* mice were purchased from Charles River Laboratory and Jackson Laboratory. All animal experiments were conducted in accordance with procedures approved by the IACUC at Cold Spring Harbor Laboratory (CSHL).

Murine pancreatic ductal organoid culture and analysis

Detailed procedures to isolate normal pancreatic ducts have been described previously (Huch et al., 2013a). In brief, normal and pre-neoplastic pancreatic ducts were manually picked after enzymatic digestion of pancreas with 0.012% (w/v) collagenase XI (Sigma) and 0.012% (w/v) dispase (Gibco) in DMEM media containing 1% FBS (Gibco), and were seeded in growth factor-reduced (GFR) Matrigel (BD). For tumors and metastases, bulk tissues were minced and digested overnight with collagenase XI and dispase and embedded in GFR Matrigel. All RNA-seq data are available at GEO under accession number GSE63348. The proteomic raw data are available at PeptideAtlas under accession number PASS00625.

Human specimens

Pancreatic cancer tissues and adjacent normal pancreas were obtained from patients undergoing surgical resection at the University Medical Centre Utrecht Hospital, Memorial Sloan-Kettering Cancer Center (MSKCC), MD Anderson Cancer Center (MDACC), and Weill Cornell Medical College (WCMC). Normal pancreatic tissue was also obtained from islet transplant programs at the University of Illinois at Chicago and University of Miami Miller School of Medicine. All human experiments were approved by the ethical committees of the University Medical Centre Utrecht or the IRBs of MSKCC, MDACC, WCMC and CSHL. Written informed consent from the donors for research use of tissue in this study was obtained prior to acquisition of the specimen. Samples were confirmed to be tumor or normal based on pathological assessment.

Human pancreatic tumor and normal organoid culture and analysis

Tumor tissue was minced and digested with collagenase II (5 mg/mL, Gibco) in human complete medium (see below) at 37°C for a maximum of 16 hours. The material was further digested with TrypLE (Gibco) for 15 minutes at 37°C, embedded in GFR Matrigel, and cultured in human complete medium [AdDMEM/F12 medium supplemented with HEPES (1x, Invitrogen), Glutamax (1x, Invitrogen), penicillin/streptomycin (1x, Invitrogen), B27 (1x, Invitrogen), Primocin (1mg/ml, InvivoGen), N-acetyl-L-cysteine (1 mM, Sigma), Wnt3a-conditioned medium (50% v/v), RSPO1-conditioned medium (10% v/v, Calvin Kuo), Noggin conditioned medium (10% v/v) or recombinant protein (0.1 μg/mL, Peprotech), epidermal growth factor (EGF, 50 ng/ml, Peprotech), Gastrin (10 nM, Sigma),

fibroblast growth factor 10 (FGF10, 100 ng/ml, Prepotech), Nicotinamide (10 mM, Sigma) and A83-01 (0.5 μM, Tocris)].

Normal samples were processed as above, except that the collagenase digestion was done for a maximum of 2 hours in the presence of soybean trypsin inhibitor (1 mg/ml, Sigma). Following digestion, cells were embedded in GFR Matrigel and cultured in human complete medium with the addition of PGE2 (1 μM, Tocris). The targeted DNA-sequencing data are available at Ensembl under the accession number ERP006373.

Additional experimental details and methods can be found in the Supplemental Extended Experimental Procedures.

Supplementary Material

Refer to Web version on PubMed Central for supplementary material.

Acknowledgments

We thank Peter Kapitein and Jan Schuurman from Inspire 2 Live for helping to establish the collaboration between DAT and HC. We also thank H. Begthel and J. Korving for technical assistance. This work was performed with assistance from the CSHL Proteomic, Histology, DNA Sequencing, Antibody, and Bioinformatics Shared Resources, which are supported by the Cancer Center Support Grant, 5P30CA045508. DAT is a distinguished scholar of the Lustgarten Foundation and Director of the Lustgarten Foundation-designated laboratory of Pancreatic Cancer Research. DAT is also supported by the Cold Spring Harbor Laboratory Association, the Carcinoid Foundation, PCUK, and the David Rubinstein Center for Pancreatic Cancer Research at MSKCC. In addition, we are grateful for support from the following – Stand Up to Cancer/KWF (HC), the STARR foundation (I7-A718 for DAT), DOD (W81XWH-13-PRCRP-IA for DAT), the Sol Goldman Pancreatic Cancer Research Center (RHH), the Italian Ministry of Health (FIRB - RBAP10AHJ for VC), Sociedad Española de Oncología Médica (SEOM for MPS), Louis Morin Charitable Trust (MEF), the Swedish Research Council (537-2013-7277 for DÖ), The Kempe Foundations (JCK-1301 for DÖ) and the Swedish Society of Medicine (SLS-326921, SLS-250831 for DÖ), the Damon Runyon Cancer Research Foundation (DRG-2165-13 for IICC), the Human Frontiers Science Program (LT000403/2014 for EE), the Weizmann Institute of Science Women in Science Award (EE), the American Cancer Society (PF-13-317-01-CSM for CMAA), the Hearst Foundation (AHS), and the NIH (5P30CA45508-26, 5P50CA101955-07, 1U10CA180944-01, 5U01CA168409-3, and 1R01CA190092-01 for DAT; CA62924 for RHH; CA134292 for SDL; 5T32CA148056 for LAB and DDE; CA101955 UAB/UMN SPORE for LAB). In addition, SFB and MH are supported by KWF/PF-HUBR 2007-3956, A.G by EU/232814-StemCellMark and RGJV by GenomiCs.nl (CGC). MJ, RB and EC are supported by the CancerGenomics.nl (NWO Gravitation) program.

References

Abbruzzese JL, Hess KR. New option for the initial management of metastatic pancreatic cancer? J Clin Oncol. 2014; 32:2405–2407. [PubMed: 24982449]

Agbunag C, Bar-Sagi D. Oncogenic K-ras drives cell cycle progression and phenotypic conversion of primary pancreatic duct epithelial cells. Cancer research. 2004; 64:5659–5663. [PubMed: 15313904]

Aguirre AJ, Bardeesy N, Sinha M, Lopez L, Tuveson DA, Horner J, Redston MS, DePinho RA. Activated Kras and Ink4a/Arf deficiency cooperate to produce metastatic pancreatic ductal adenocarcinoma. Genes Dev. 2003; 17:3112–3126. [PubMed: 14681207]

Bardeesy N, Aguirre AJ, Chu GC, Cheng KH, Lopez LV, Hezel AF, Feng B, Brennan C, Weissleder R, Mahmood U, et al. Both p16(Ink4a) and the p19(Arf)-p53 pathway constrain progression of pancreatic adenocarcinoma in the mouse. Proc Natl Acad Sci U S A. 2006; 103:5947–5952. [PubMed: 16585505]

Barker N, Huch M, Kujala P, van de Wetering M, Snippert HJ, van Es JH, Sato T, Stange DE, Begthel H, van den Born M, et al. Lgr5(+ve) stem cells drive self-renewal in the stomach and build long-lived gastric units in vitro. Cell Stem Cell. 2010; 6:25–36. [PubMed: 20085740]

Beatty GL, Chiorean EG, Fishman MP, Saboury B, Teitelbaum UR, Sun W, Huhn RD, Song W, Li D, Sharp LL, et al. CD40 agonists alter tumor stroma and show efficacy against pancreatic carcinoma in mice and humans. Science. 2011; 331:1612–1616. [PubMed: 21436454]

Cheung HW, Cowley GS, Weir BA, Boehm JS, Rusin S, Scott JA, East A, Ali LD, Lizotte PH, Wong TC, et al. Systematic investigation of genetic vulnerabilities across cancer cell lines reveals lineage-specific dependencies in ovarian cancer. Proc Natl Acad Sci U S A. 2011; 108:12372–12377. [PubMed: 21746896]

Cleveland MH, Sawyer JM, Afelik S, Jensen J, Leach SD. Exocrine ontogenies: On the development of pancreatic acinar, ductal and centroacinar cells. Seminars in Cell & Developmental Biology. 2012; 23:711–719. [PubMed: 22743232]

De La OJ, Emerson LL, Goodman JL, Froebe SC, Illum BE, Curtis AB, Murtaugh LC. Notch and Kras reprogram pancreatic acinar cells to ductal intraepithelial neoplasia. Proc Natl Acad Sci U S A. 2008; 105:18907–18912. [PubMed: 19028876]

DeNicola GM, Karreth FA, Humpton TJ, Gopinathan A, Wei C, Frese K, Mangal D, Yu KH, Yeo CJ, Calhoun ES, et al. Oncogene-induced Nrf2 transcription promotes ROS detoxification and tumorigenesis. Nature. 2011; 475:106–109. [PubMed: 21734707]

Dumartin L, Whiteman HJ, Weeks ME, Hariharan D, Dmitrovic B, Iacobuzio-Donahue CA, Brentnall TA, Bronner MP, Feakins RM, Timms JF, et al. AGR2 is a novel surface antigen that promotes the dissemination of pancreatic cancer cells through regulation of cathepsins B and D. Cancer research. 2011; 71:7091–7102. [PubMed: 21948970]

Erkan M, Reiser-Erkan C, Michalski CW, Deucker S, Sauliunaite D, Streit S, Esposito I, Friess H, Kleeff J. Cancer-stellate cell interactions perpetuate the hypoxia-fibrosis cycle in pancreatic ductal adenocarcinoma. Neoplasia. 2009; 11:497–508. [PubMed: 19412434]

Feig C, Jones JO, Kraman M, Wells RJ, Deonarine A, Chan DS, Connell CM, Roberts EW, Zhao Q, Caballero OL, et al. Targeting CXCL12 from FAP-expressing carcinoma-associated fibroblasts synergizes with anti-PD-L1 immunotherapy in pancreatic cancer. Proc Natl Acad Sci U S A. 2013; 110:20212–20217. [PubMed: 24277834]

Frese KK, Neesse A, Cook N, Bapiro TE, Lolkema MP, Jodrell DI, Tuveson DA. nab-Paclitaxel potentiates gemcitabine activity by reducing cytidine deaminase levels in a mouse model of pancreatic cancer. Cancer Discov. 2012; 2:260–269. [PubMed: 22585996]

Gao D, Vela I, Sboner A, Iaquinta PJ, Karthaus WR, Gopalan A, Dowling C, Wanjala JN, Undvall EA, Arora VK, et al. Organoid cultures derived from patients with advanced prostate cancer. Cell. 2014; 159:176–187. [PubMed: 25201530]

Gidekel Friedlander SY, Chu GC, Snyder EL, Girnius N, Dibelius G, Crowley D, Vasile E, DePinho RA, Jacks T. Context-dependent transformation of adult pancreatic cells by oncogenic K-Ras. Cancer Cell. 2009; 16:379–389. [PubMed: 19878870]

Gould VE, Martinez N, Orucevic A, Schneider J, Alonso A. A novel, nuclear pore-associated, widely distributed molecule overexpressed in oncogenesis and development. Am J Pathol. 2000; 157:1605–1613. [PubMed: 11073820]

Guerra C, Mijimolle N, Dhawahir A, Dubus P, Barradas M, Serrano M, Campuzano V, Barbacid M. Tumor induction by an endogenous K-ras oncogene is highly dependent on cellular context. Cancer Cell. 2003; 4:111–120. [PubMed: 12957286]

Habbe N, Shi G, Meguid RA, Fendrich V, Esni F, Chen H, Feldmann G, Stoffers DA, Konieczny SF, Leach SD, et al. Spontaneous induction of murine pancreatic intraepithelial neoplasia (mPanIN) by acinar cell targeting of oncogenic Kras in adult mice. Proc Natl Acad Sci U S A. 2008; 105:18913–18918. [PubMed: 19028870]

Hingorani SR, Petricoin EF, Maitra A, Rajapakse V, King C, Jacobetz MA, Ross S, Conrads TP, Veenstra TD, Hitt BA, et al. Preinvasive and invasive ductal pancreatic cancer and its early detection in the mouse. Cancer Cell. 2003; 4:437–450. [PubMed: 14706336]

Hingorani SR, Wang L, Multani AS, Combs C, Deramaudt TB, Hruban RH, Rustgi AK, Chang S, Tuveson DA. Trp53R172H and KrasG12D cooperate to promote chromosomal instability and widely metastatic pancreatic ductal adenocarcinoma in mice. Cancer Cell. 2005; 7:469–483. [PubMed: 15894267]

Huch M, Bonfanti P, Boj SF, Sato T, Loomans CJ, van de Wetering M, Sojoodi M, Li VS, Schuijers J, Gracanin A, et al. Unlimited in vitro expansion of adult bi-potent pancreas progenitors through the Lgr5/R-spondin axis. Embo J. 2013a:2708–2721. [PubMed: 24045232]

Huch M, Dorrell C, Boj SF, van Es JH, Li VS, van de Wetering M, Sato T, Hamer K, Sasaki N, Finegold MJ, et al. In vitro expansion of single Lgr5+ liver stem cells induced by Wnt-driven regeneration. Nature. 2013b; 494:247–250. [PubMed: 23354049]

Jacobetz MA, Chan DS, Neesse A, Bapiro TE, Cook N, Frese KK, Feig C, Nakagawa T, Caldwell ME, Zecchini HI, et al. Hyaluronan impairs vascular function and drug delivery in a mouse model of pancreatic cancer. Gut. 2012:112–120. [PubMed: 22466618]

Karthaus WR, Iaquinta PJ, Drost J, Gracanin A, van Boxtel R, Wongvipat J, Dowling CM, Gao D, Begthel H, Sachs N, et al. Identification of multipotent luminal progenitor cells in human prostate organoid cultures. Cell. 2014; 159:163–175. [PubMed: 25201529]

Kim J, Hoffman John P, Alpaugh RK, Rhim Andrew D, Reichert M, Stanger Ben Z, Furth Emma E, Sepulveda Antonia R, Yuan CX, Won KJ, et al. An iPSC Line from Human Pancreatic Ductal Adenocarcinoma Undergoes Early to Invasive Stages of Pancreatic Cancer Progression. Cell Rep. 2013; 3:2088–2099. [PubMed: 23791528]

Kim MP, Evans DB, Wang H, Abbruzzese JL, Fleming JB, Gallick GE. Generation of orthotopic and heterotopic human pancreatic cancer xenografts in immunodeficient mice. Nat Protoc. 2009; 4:1670–1680. [PubMed: 19876027]

Kohler A, Hurt E. Gene regulation by nucleoporins and links to cancer. Mol Cell. 2010; 38:6–15. [PubMed: 20385085]

Koong AC, Mehta VK, Le QT, Fisher GA, Terris DJ, Brown JM, Bastidas AJ, Vierra M. Pancreatic tumors show high levels of hypoxia. Int J Radiat Oncol Biol Phys. 2000; 48:919–922. [PubMed: 11072146]

Kopp JL, von Figura G, Mayes E, Liu FF, Dubois CL, Morris JPt, Pan FC, Akiyama H, Wright CV, Jensen K, et al. Identification of Sox9-dependent acinar-to-ductal reprogramming as the principal mechanism for initiation of pancreatic ductal adenocarcinoma. Cancer Cell. 2012; 22:737–750. [PubMed: 23201164]

Lee J, Sugiyama T, Liu Y, Wang J, Gu X, Lei J, Markmann JF, Miyazaki S, Miyazaki J, Szot GL, et al. Expansion and conversion of human pancreatic ductal cells into insulin-secreting endocrine cells. eLife. 2013; 2:e00940. [PubMed: 24252877]

Li X, Nadauld L, Ootani A, Corney DC, Pai RK, Gevaert O, Cantrell MA, Rack PG, Neal JT, Chan CW, et al. Oncogenic transformation of diverse gastrointestinal tissues in primary organoid culture. Nat Med. 2014; 20:769–777. [PubMed: 24859528]

Makovitzky J. The distribution and localization of the monoclonal antibody-defined antigen 19-9 (CA19-9) in chronic pancreatitis and pancreatic carcinoma. An immunohistochemical study. Virchows Archiv B, Cell pathology including molecular pathology. 1986; 51:535–544.

Means AL, Meszoely IM, Suzuki K, Miyamoto Y, Rustgi AK, Coffey RJ, Wright CVE, Stoffers DA, Leach SD. Pancreatic epithelial plasticity mediated by acinar cell transdifferentiation and generation of nestin-positive intermediates. Development. 2005; 132:3767–3776. [PubMed: 16020518]

Morris, JPt; Cano, DA.; Sekine, S.; Wang, SC.; Hebrok, M. Beta-catenin blocks Kras-dependent reprogramming of acini into pancreatic cancer precursor lesions in mice. J Clin Invest. 2010; 120:508–520. [PubMed: 20071774]

Neesse A, Frese KK, Chan DS, Bapiro TE, Howat WJ, Richards FM, Ellenrieder V, Jodrell DI, Tuveson DA. SPARC independent drug delivery and antitumour effects of nab-paclitaxel in genetically engineered mice. Gut. 2014; 63:974–983. [PubMed: 24067278]

Olive KP, Jacobetz MA, Davidson CJ, Gopinathan A, McIntyre D, Honess D, Madhu B, Goldgraben MA, Caldwell ME, Allard D, et al. Inhibition of Hedgehog signaling enhances delivery of chemotherapy in a mouse model of pancreatic cancer. Science. 2009; 324:1457–1461. [PubMed: 19460966]

Perez-Mancera PA, Guerra C, Barbacid M, Tuveson DA. What We Have Learned About Pancreatic Cancer from Mouse Models. Gastroenterology. 2012:1079–1092. [PubMed: 22406637]

Prasad NB, Biankin AV, Fukushima N, Maitra A, Dhara S, Elkahloun AG, Hruban RH, Goggins M, Leach SD. Gene expression profiles in pancreatic intraepithelial neoplasia reflect the effects of Hedgehog signaling on pancreatic ductal epithelial cells. Cancer research. 2005; 65:1619–1626. [PubMed: 15753353]

Provenzano PP, Cuevas C, Chang AE, Goel VK, Von Hoff DD, Hingorani SR. Enzymatic targeting of the stroma ablates physical barriers to treatment of pancreatic ductal adenocarcinoma. Cancer Cell. 2012; 21:418–429. [PubMed: 22439937]

Pylayeva-Gupta Y, Lee KE, Hajdu CH, Miller G, Bar-Sagi D. Oncogenic Kras-induced GM-CSF production promotes the development of pancreatic neoplasia. Cancer Cell. 2012; 21:836–847. [PubMed: 22698407]

Rahib L, Smith BD, Aizenberg R, Rosenzweig AB, Fleshman JM, Matrisian LM. Projecting cancer incidence and deaths to 2030: the unexpected burden of thyroid, liver, and pancreas cancers in the United States. Cancer Res. 2014; 74:2913–2921. [PubMed: 24840647]

Ray KC, Bell KM, Yan J, Gu G, Chung CH, Washington MK, Means AL. Epithelial tissues have varying degrees of susceptibility to Kras(G12D)-initiated tumorigenesis in a mouse model. PLoS One. 2011; 6:e16786. [PubMed: 21311774]

Rovira M, Scott SG, Liss AS, Jensen J, Thayer SP, Leach SD. Isolation and characterization of centroacinar/terminal ductal progenitor cells in adult mouse pancreas. Proc Natl Acad Sci U S A. 2010; 107:75–80. [PubMed: 20018761]

Rubio-Viqueira B, Jimeno A, Cusatis G, Zhang X, Iacobuzio-Donahue C, Karikari C, Shi C, Danenberg K, Danenberg PV, Kuramochi H, et al. An in vivo platform for translational drug development in pancreatic cancer. Clinical cancer research: an official journal of the American Association for Cancer Research. 2006; 12:4652–4661. [PubMed: 16899615]

Ryan DP, Hong TS, Bardeesy N. Pancreatic adenocarcinoma. N Engl J Med. 2014; 371:1039–1049. [PubMed: 25207767]

Sato T, Stange DE, Ferrante M, Vries RG, Van Es JH, Van den Brink S, Van Houdt WJ, Pronk A, Van Gorp J, Siersema PD, et al. Long-term expansion of epithelial organoids from human colon, adenoma, adenocarcinoma, and Barrett's epithelium. Gastroenterology. 2011; 141:1762–1772. [PubMed: 21889923]

Sato T, Vries RG, Snippert HJ, van de Wetering M, Barker N, Stange DE, van Es JH, Abo A, Kujala P, Peters PJ, et al. Single Lgr5 stem cells build crypt-villus structures in vitro without a mesenchymal niche. Nature. 2009; 459:262–265. [PubMed: 19329995]

Sawey ET, Johnson JA, Crawford HC. Matrix metalloproteinase 7 controls pancreatic acinar cell transdifferentiation by activating the Notch signaling pathway. Proc Natl Acad Sci U S A. 2007; 104:19327–19332. [PubMed: 18042722]

Seaberg RM, Smukler SR, Kieffer TJ, Enikolopov G, Asghar Z, Wheeler MB, Korbutt G, van der Kooy D. Clonal identification of multipotent precursors from adult mouse pancreas that generate neural and pancreatic lineages. Nat Biotechnol. 2004; 22:1115–1124. [PubMed: 15322557]

Shain AH, Salari K, Giacomini CP, Pollack JR. Integrative genomic and functional profiling of the pancreatic cancer genome. BMC genomics. 2013; 14:624. [PubMed: 24041470]

Sharma SV, Haber DA, Settleman J. Cell line-based platforms to evaluate the therapeutic efficacy of candidate anticancer agents. Nat Rev Cancer. 2010; 10:241–253. [PubMed: 20300105]

Siegel R, Naishadham D, Jemal A. Cancer statistics, 2013. CA Cancer J Clin. 2013; 63:11–30. [PubMed: 23335087]

Subramanian A, Tamayo P, Mootha VK, Mukherjee S, Ebert BL, Gillette MA, Paulovich A, Pomeroy SL, Golub TR, Lander ES, et al. Gene set enrichment analysis: a knowledge-based approach for interpreting genome-wide expression profiles. Proc Natl Acad Sci U S A. 2005; 102:15545–15550. [PubMed: 16199517]

Villarroel MC, Rajeshkumar NV, Garrido-Laguna I, De Jesus-Acosta A, Jones S, Maitra A, Hruban RH, Eshleman JR, Klein A, Laheru D, et al. Personalizing cancer treatment in the age of global genomic analyses: PALB2 gene mutations and the response to DNA damaging agents in pancreatic cancer. Mol Cancer Ther. 2011; 10:3–8. [PubMed: 21135251]

von Figura G, Fukuda A, Roy N, Liku ME, Morris JP IV, Kim GE, Russ HA, Firpo MA, Mulvihill SJ, Dawson DW, et al. The chromatin regulator Brg1 suppresses formation of intraductal papillary

mucinous neoplasm and pancreatic ductal adenocarcinoma. Nat Cell Biol. 2014; 16:255–267. [PubMed: 24561622]

Wiese S, Reidegeld KA, Meyer HE, Warscheid B. Protein labeling by iTRAQ: a new tool for quantitative mass spectrometry in proteome research. Proteomics. 2007; 7:340–350. [PubMed: 17177251]

Ying H, Kimmelman AC, Lyssiotis CA, Hua S, Chu GC, Fletcher-Sananikone E, Locasale JW, Son J, Zhang H, Coloff JL, et al. Oncogenic Kras maintains pancreatic tumors through regulation of anabolic glucose metabolism. Cell. 2012; 149:656–670. [PubMed: 22541435]

Zhao LL, Zhang T, Liu BR, Liu TF, Tao N, Zhuang LW. Construction of pancreatic cancer double-factor regulatory network based on chip data on the transcriptional level. Molecular biology reports. 2014; 41:2875–2883. [PubMed: 24469724]

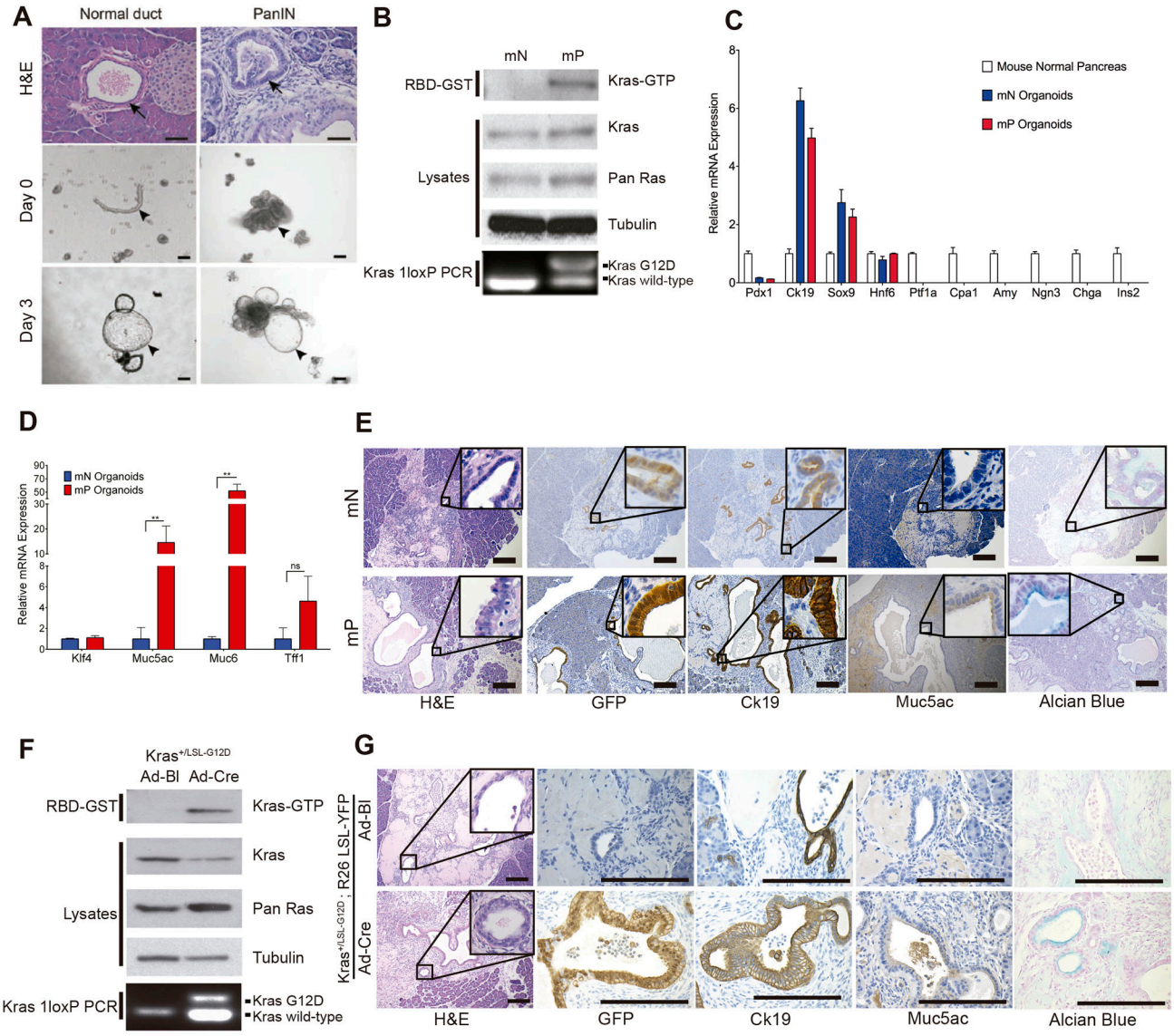

Figure 1. Oncogenic *Kras*^{G12D} expression in pancreatic ductal organoids is sufficient to induce pre-invasive neoplasms

(A) Hematoxylin and eosin (H&E) staining of murine pancreatic tissue used to prepare organoids (top). Arrows indicate mouse normal or PanIN ductal structures. Ducts embedded in Matrigel immediately following isolation (middle) and organoids 3 days post-isolation (bottom). Arrowheads mark isolated ducts and growing organoids. Scale bars, 50 μm.

(B) Immunoblots for Kras, pan-Ras, Kras-GTP by RBD-GST pull-down and Tubulin in mouse normal (mN) and mPanIN (mP) organoids. PCR confirmation of Cre-mediated recombination of the *Kras*$^{LSL-G12D}$ allele (bottom).

(C) qRT-PCR of ductal (*Pdx1*, *Ck19*, *Sox9*, *Hnf6*), acinar (*Ptf1a*, *Cpa1*, *Amy*), and endocrine (*Ngn3*, *Chga*, *Ins2*) lineage markers in mN and mP organoids. Means of 3 biological replicates are shown. Error bars depict standard error of the means (SEMs). Values were normalized to mouse normal pancreas.

(D) qRT-PCR of genes indicative of PanIN lesions (*Muc5ac*, *Muc6*, *Tff1*, *Klf4*) in mN and mP organoids. Values were normalized to mN organoids. Means of 3 biological replicates are shown. Error bars depict SEMs. **: $p < 0.01$ by two-tailed Student's *t*-test.
(E) H&E, Alcian Blue staining, and immunohistochemistry (IHC) of orthotopic, syngeneic transplants of GFP-transduced mN and mP organoids. Scale bars, 200 μm.
(F) Immunoblots for Kras, pan-Ras, Kras-GTP by RBD-GST pull-down and Tubulin in $Kras^{+/LSL\text{-}G12D}$ organoids transduced with adenoviral-Cre (Ad-Cre) or adenoviral-blank (Ad-Bl). PCR confirmation of Cre-mediated recombination of the $Kras^{LSL\text{-}G12D}$ allele (bottom).
(G) H&E, Alcian Blue staining, and IHC of orthotopic syngeneic transplants of organoids transduced with Ad-Bl ($Kras^{+/LSL\text{-}G12D}$; *R26-LSL-YFP*) and Ad-Cre ($Kras^{+/LSL\text{-}G12D}$; *R26-YFP*) 2 weeks post-transplant. Scale bars, 200 μm.
See also Figure S1 and Table S1.

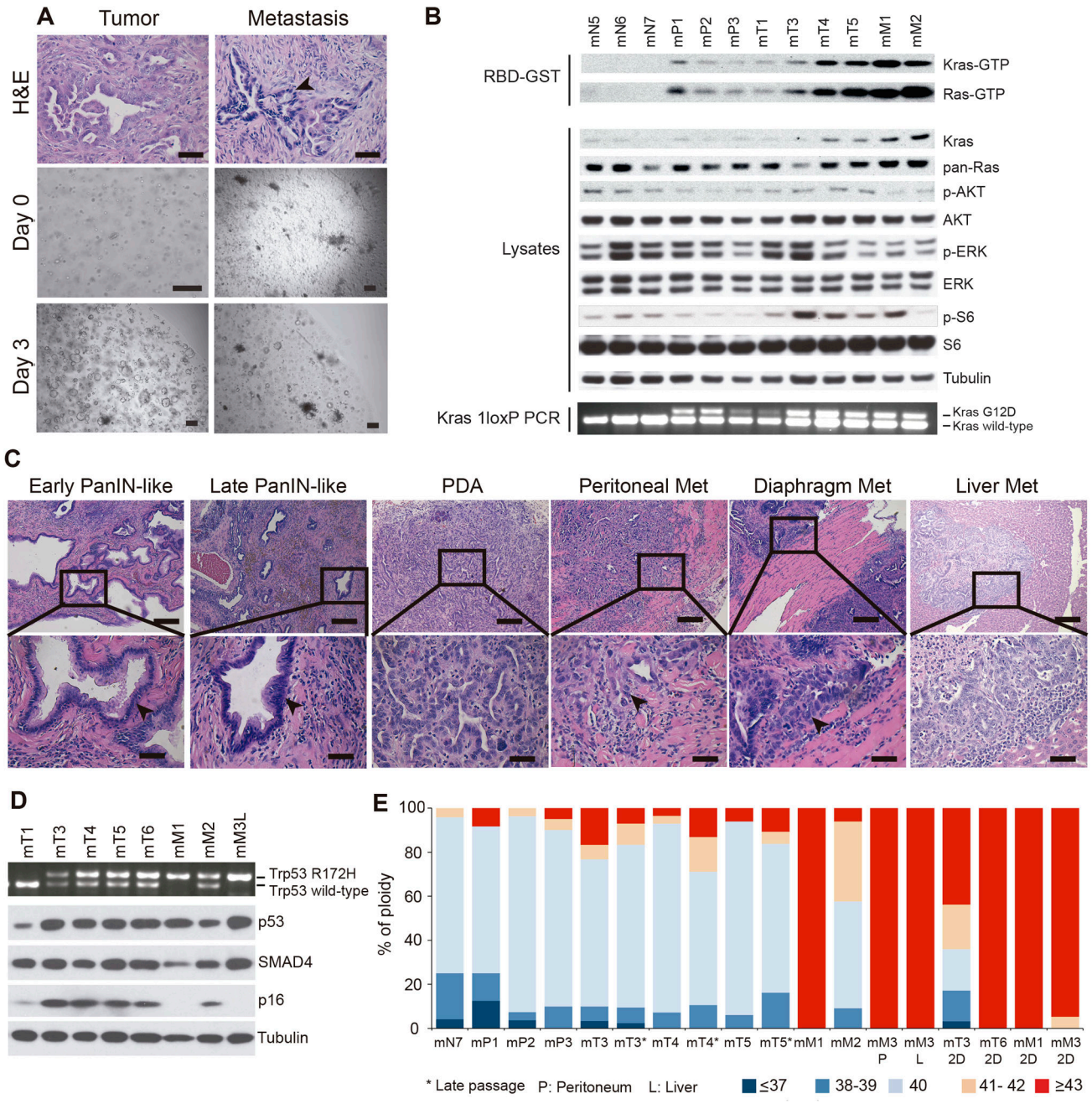

Figure 2. Modeling murine PDA progression with tumor- and metastasis-derived organoids

(A) H&E staining of murine tissue from which tumor and metastasis organoids were derived (top). Arrowhead indicates metastasis. Scale bars, 50 μm. Digested murine tissues embedded in Matrigel immediately following isolation (middle) and organoids 3 days post-isolation (bottom). Scale bars, 200 μm.

(B) Immunoblots of selected signaling effectors, Kras-GTP and Ras-GTP by RBD-GST pull-down, and Tubulin. PCR confirmation of *Kras*$^{LSL\text{-}G12D}$ recombination in mP, mT, and mM organoids (bottom).

(C) H&E staining of tumors and metastases (met) derived from mT organoid orthotopic transplants. Scale bars, 200 μm (top) and 50 μm (bottom).
(D) Loss of heterozygosity of the wild-type *Trp53* allele determined by PCR (top) and immunoblot analysis of Trp53, Smad4, and p16, and Tubulin. mM3L: derived from a liver metastasis.
(E) Karyotypes of organoids and monolayer (2D) cell lines.
See also Figure S2 and Table S2.

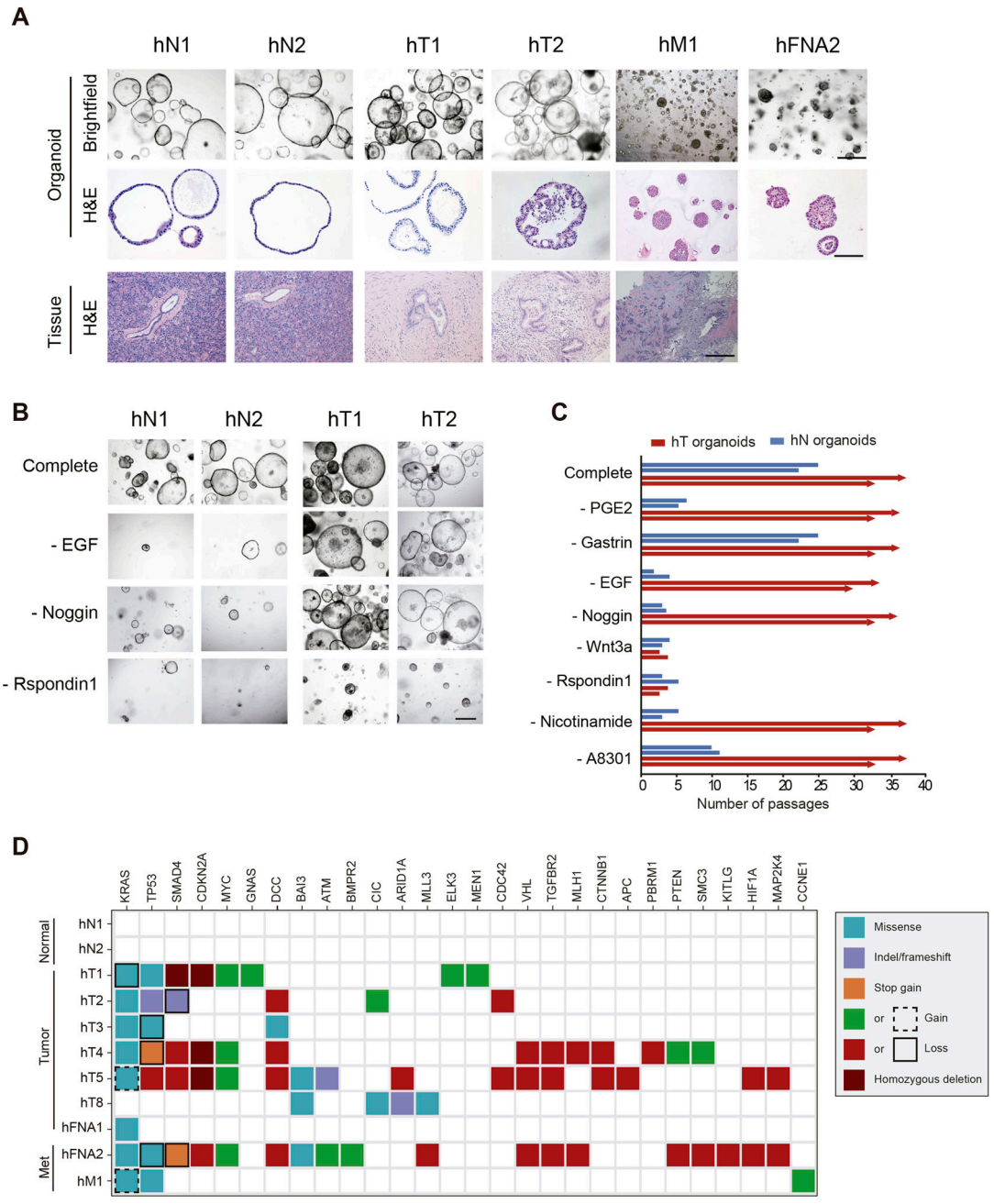

Figure 3. Human pancreatic ductal organoids recapitulate features of normal and neoplastic ducts

(A) Representative images (top) and H&E staining (middle) of human organoid cultures established from: normal tissues (hN1-2), resected primary tumors (hT1-2), a resected metastatic lung lesion (hM1) and a fine-needle aspiration biopsy of a metastatic lesion (hFNA2). H&E staining of the resected tissues from which the organoids were derived (bottom). Scale bars, 500 μm (top), 250 μm (middle), and 500 μm (bottom).

(B) Representative images of hN and hT organoids cultured for two weeks (1 passage) in human complete media, or in human complete media lacking the indicated factors. Scale bars, 500 μm.

(C) Number of passages hN and hT organoids could be propagated in the absence of the indicated factors.

(D) Targeted sequencing analysis of human organoids. Genes altered in more than one sample and/or known to be mutated in PDA are shown. If multiple mutations were found in a gene, only one mutation per gene is shown. Color key for the type of genetic alterations is shown. Met indicates organoids derived from metastatic samples.

See also Figure S3, Table S3 and S4

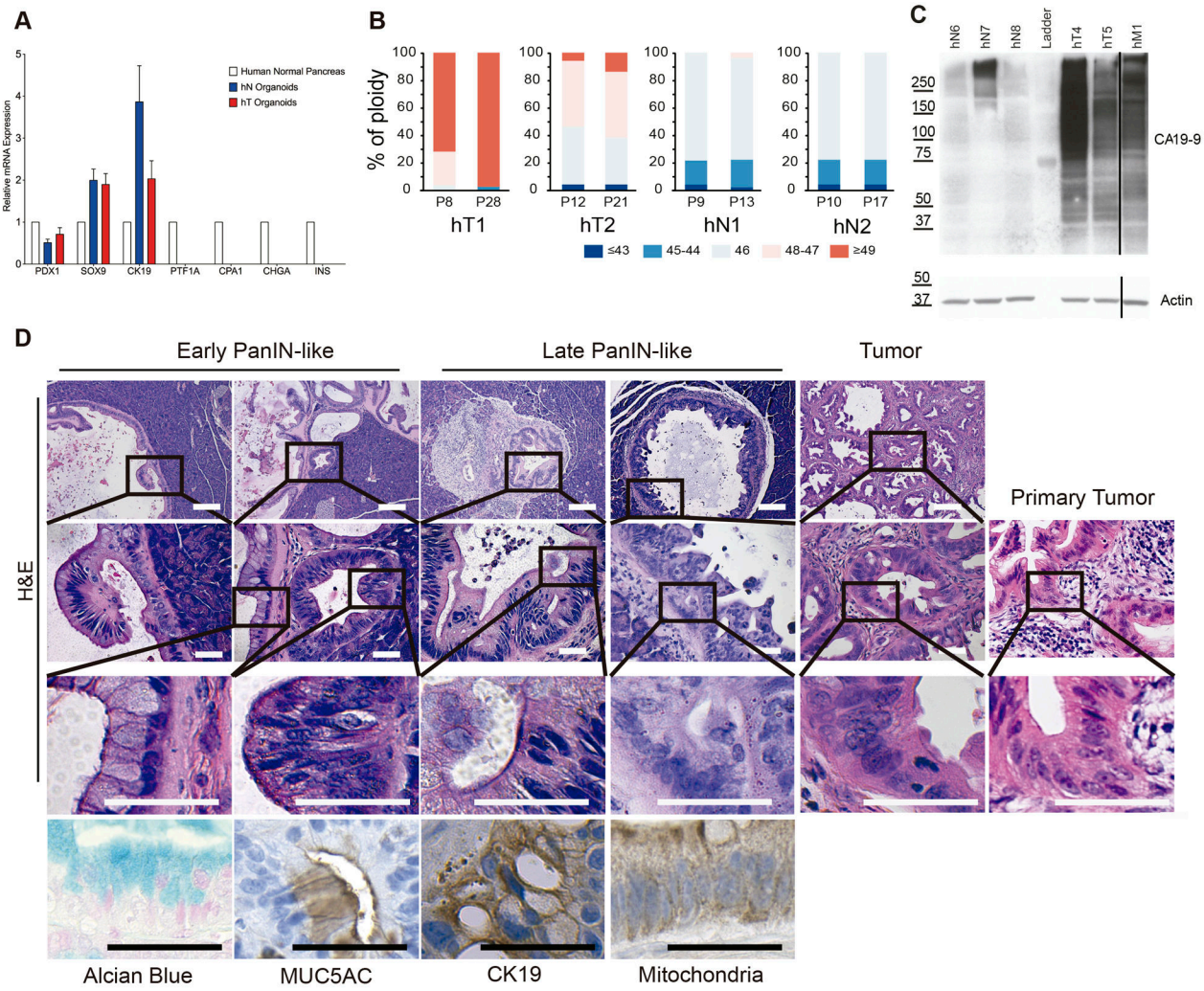

Figure 4. Molecular characterization and orthotopic transplantation of human organoids

(A) qRT-PCR of pancreas lineage markers in hN (n = 3) and hT (n = 4) organoids. Mean expression levels were normalized to total pancreas. Error bars depict SEMs.

(B) Karyotyping of human organoids (2 hN, 2hT) at the indicated passages (P).

(C) CA19-9 and actin levels in hN, hT, or hM organoids. The solid line indicates non-congruent lanes.

(D) H&E, Alcian Blue staining and IHC of orthotopic hT2 transplants and the primary tumor. Scale bars, 200 μm (top two panels) and 50 μm (lower two panels).

See also Figure S4 and Table S4D

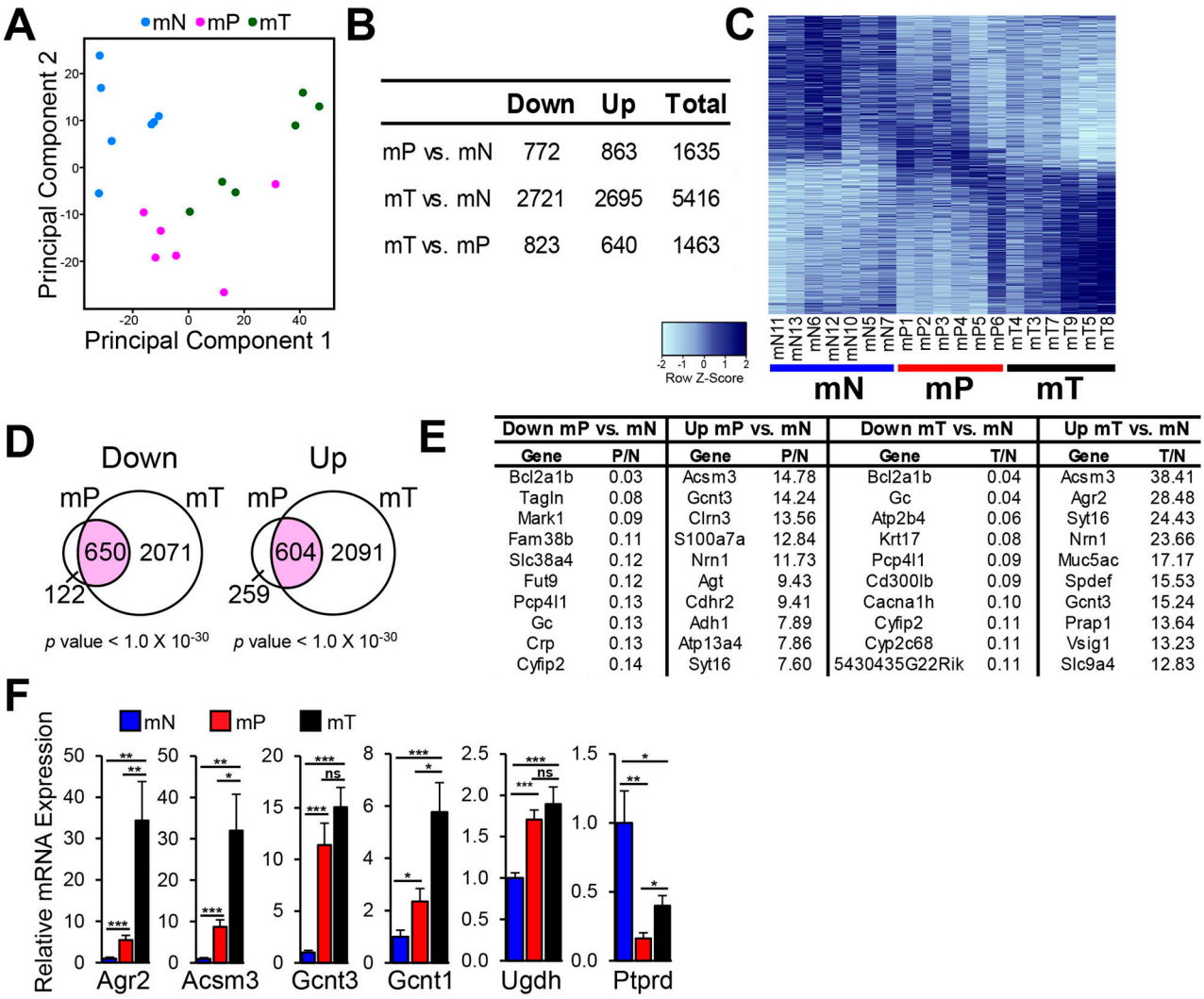

	Down	Up	Total
mP vs. mN	772	863	1635
mT vs. mN	2721	2695	5416
mT vs. mP	823	640	1463

Down mP vs. mN		Up mP vs. mN		Down mT vs. mN		Up mT vs. mN	
Gene	P/N	Gene	P/N	Gene	T/N	Gene	T/N
Bcl2a1b	0.03	Acsm3	14.78	Bcl2a1b	0.04	Acsm3	38.41
Tagln	0.08	Gcnt3	14.24	Gc	0.04	Agr2	28.48
Mark1	0.09	Clrn3	13.56	Atp2b4	0.06	Syt16	24.43
Fam38b	0.11	S100a7a	12.84	Krt17	0.08	Nrn1	23.66
Slc38a4	0.12	Nrn1	11.73	Pcp4l1	0.09	Muc5ac	17.17
Fut9	0.12	Agt	9.43	Cd300lb	0.09	Spdef	15.53
Pcp4l1	0.13	Cdhr2	9.41	Cacna1h	0.10	Gcnt3	15.24
Gc	0.13	Adh1	7.89	Cyfip2	0.11	Prap1	13.64
Crp	0.13	Atp13a4	7.86	Cyp2c68	0.11	Vsig1	13.23
Cyfip2	0.14	Syt16	7.60	5430435G22Rik	0.11	Slc9a4	12.83

Figure 5. Gene expression analysis of murine organoids reveals genetic changes correlated with pancreatic cancer progression

(A) Principal component analysis of gene expression data for mN, mP, and mT organoids.

(B) The number of genes differentially expressed (DESeq adjusted *p* value < 0.05) among mN (n = 7), mP (n = 6), and mT (n = 6) organoids.

(C) Heatmap showing relative expression levels using Z-score normalization among mN, mP, and mT organoids. Color key of Z-score is shown.

(D) Venn diagrams show overlap of genes significantly differentially expressed in mP and mT relative to mN organoids. The *p* values for overlaps were determined by two-tailed Fisher's Exact test.

(E) Genes with the largest fold-changes in mP or mT relative to mN organoids.

(F) qRT-PCR validation of mN, mP and mT organoid gene expression changes. Values were normalized to mean levels in mN organoids. n = 8 mN, 7 mP, and 8 mT organoid cultures. Error bars show SEMs. *, **, ***, ns: $p < 0.05$, 0.01, 0.001, or not significant by two-tailed Student's *t*-test.

See also Figure S5 and Table S5.

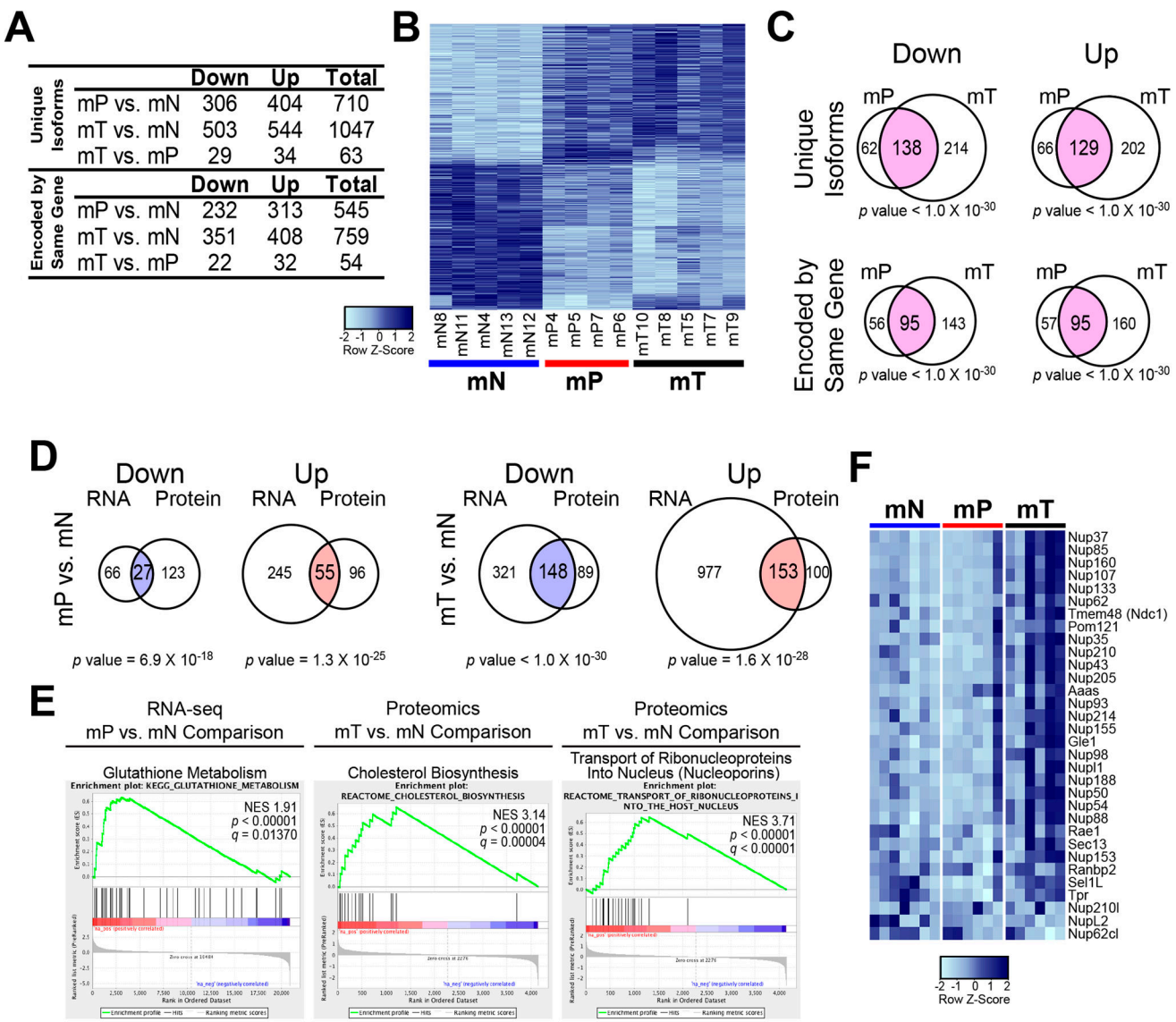

Figure 6. Proteomic profiling of murine organoids uncovers molecular pathways linked to pancreatic cancer progression

(A) Protein expression changes by iTRAQ proteomic analysis of murine organoids. Both unique protein isoforms and protein isoforms encoded by the same gene are included (adjusted *p* value < 0.1 by linear regression analysis).

(B) Heatmap of unique protein isoforms that differ (adjusted *p* value < 0.05) among mN, mP, and mT organoids. Color key of the Z-score is shown.

(C) Venn diagrams showing overlaps between proteins differentially expressed ($p < 0.05$) in mP and mT relative to mN organoids. *p* values for overlaps were determined by two-tailed Fisher's Exact test.

(D) Venn diagrams showing overlaps between genes and proteins found differentially expressed by RNA-seq and proteomic analyses (adjusted $p < 0.05$). *p* values for the overlaps were determined by two-tailed Fisher's Exact test.

(E) Molecular pathways found enriched by GSEA analysis of RNA-seq and proteomic data. Normalized enrichment scores (NESs), *p* and *q* values are shown.

(F) Heatmap showing relative gene expression levels of nucleoporins in mN, mP, and mT organoids determined by RNA-seq. Color key of the Z-score is shown.

See also Figure S6, Table S6 and S7.

A

Gene name	Mouse normal duct	mPanIN	mPDA
ACSM3	+	++	+++
NT5E	-	++	+++
UGDH	-	+	+++
GCNT1	-	+++	++
GCNT3	+	++	++
FGF1	-	++	++
AGT	-	+	++
TNS4	+	++	+++
LIN28	+	+++	++
ADH1	-	+	++
DDC	-	+	++
PCSK6	-	+	+
GCAT	+++	++	++
AGR2	+	+++	+++

B

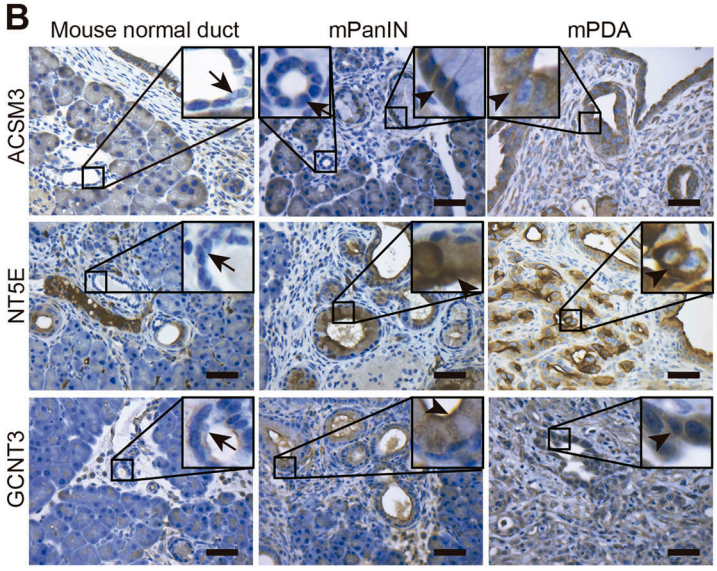

C

Gene name	Human normal duct	Human PDA	hT Transplants
ACSM3	+	+++	+++
NT5E	+	+++	+++
GCNT3	+	+++	++
UGDH	-	+++	+++
GCNT1	+	++	+
ADH1	++	+++	+
TNS4	+	+++	++

D

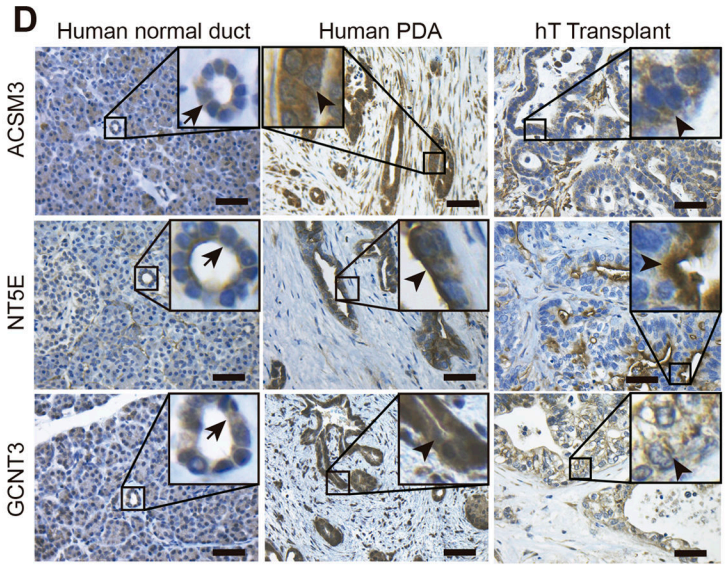

Figure 7. Increased levels of ACSM3, NT5E and GCNT3 correlate with mouse and human PDA progression

(A) IHC analysis of 14 candidate genes in mouse adjacent normal ducts, mPanlN and mPDA. Differential expression is indicated as: - (negative), + (weak), ++ (moderate) or +++ (strong).

(B) IHC analysis of ACSM3, NT5E and GCNT3 in mouse normal ducts, mPanlN and mPDA tissues. Arrow indicates adjacent normal ducts in mPanlN tissues. Arrowhead indicates mPanlN or mPDA. Scale bars, 50 μm.

(C) IHC analysis of 7 candidate genes in human normal pancreas, hT orthotopic transplants and PDA tissues. Differential expression is indicated as: - (negative), + (weak), ++ (moderate) or +++ (strong). Only the ductal component of the normal pancreas was scored.

(D) IHC analysis of ACSM3, NT5E and GCNT3 in human normal pancreas and PDA tissues. Arrow indicates normal ducts and arrowhead indicates PDA. Scale bars, 50 μm.

See also Figure S7.